



TIL in baroclinic life cycle experiments

D. Kunkel et al.

This discussion paper is/has been under review for the journal Atmospheric Chemistry and Physics (ACP). Please refer to the corresponding final paper in ACP if available.

The tropopause inversion layer in baroclinic life cycles experiments: the role of diabatic and mixing processes

D. Kunkel, P. Hoor, and V. Wirth

Institute for Atmospheric Physics, Johannes-Gutenberg University Mainz, Mainz, Germany

Received: 21 July 2015 – Accepted: 27 July 2015 – Published: 10 August 2015

Correspondence to: D. Kunkel (dkunkel@uni-mainz.de)

Published by Copernicus Publications on behalf of the European Geosciences Union.

Title Page

Abstract

Introduction

Conclusions

References

Tables

Figures



Back

Close

Full Screen / Esc

Printer-friendly Version

Interactive Discussion



Abstract

Recent studies on the formation of a quasi-permanent layer of enhanced static stability above the thermal tropopause revealed the contributions of dynamical and radiative processes. Dry dynamics lead to the evolution of a tropopause inversion layer (TIL) which is, however, too weak compared to observations and thus diabatic contributions are required. In this study we aim to assess the importance of diabatic as well as mixing processes in the understanding of TIL formation at midlatitudes. The non-hydrostatic model COSMO is applied in an idealized mid-latitude channel configuration to simulate baroclinic life cycles. The effect of individual diabatic, i.e. related to humidity and radiation, and turbulent processes is studied first to estimate the additional contribution of these processes to dry dynamics. In a second step these processes are stepwise included in the model to increase the complexity and finally estimate the relative importance of each process. The results suggest that including turbulence leads to a weaker TIL than in a dry reference simulation. In contrast, the TIL evolves stronger when radiation is included but the temporal occurrence is still comparable to the reference. Using various cloud schemes in the model shows that latent heat release and consecutive increased vertical motions foster an earlier and stronger appearance of the TIL than in all other life cycles. Furthermore, updrafts moisten the upper troposphere and as such increase the radiative effect from water vapor. Particularly, this process becomes more relevant for maintaining the TIL during later stages of the life cycles. Increased convergence of the vertical wind induced by updrafts and by propagating and potentially dissipating inertia-gravity waves further contributes to the enhanced stability of the lower stratosphere. Furthermore, radiative feedback of ice clouds reaching up to the tropopause is identified to potentially further affect the strength of the TIL in the region of the cloud.

TIL in baroclinic life cycle experiments

D. Kunkel et al.

Title Page

Abstract

Introduction

Conclusions

References

Tables

Figures



Back

Close

Full Screen / Esc

Printer-friendly Version

Interactive Discussion



1 Introduction

The sharpness of the tropopause in the extratropics has gained increased attention in recent years (e.g., Gettelman and Wang, 2015). Local maxima of static stability, usually measured by the squared Brunt–Vaisala frequency $N^2 = g/\Theta \cdot \partial\Theta/\partial z$ with g , the gravitational acceleration, Θ , the potential temperature, and z , the geometric altitude, inferred from radiosonde measurements (e.g., Birner et al., 2002; Birner, 2006) and Global Positioning System (GPS) radio occultation measurements (Randel et al., 2007), revealed the existence of a quasi-permanent inversion layer above the thermal tropopause. This tropopause inversion layer (TIL) is a distinct feature of the region of the upper troposphere and lower stratosphere (UTLS), from tropical to polar regions (e.g., Grise et al., 2010) and is also evident in general circulation models and climate analysis data sets (e.g., Birner et al., 2006).

Global studies of GPS temperature profiles and reanalysis data sets showed that the TIL is present at all latitudes (Grise et al., 2010; Gettelman and Wang, 2015). In the tropical lower stratosphere two maxima of enhanced static stability are found at about 17 and 19 km altitude. The upper peak shows a seasonal cycle with a winter maximum, while the lower peak has relatively large values all year round (Grise et al., 2010). In polar regions a distinct summer maximum occurs (Randel and Wu, 2010), while the TIL is evident in midlatitudes throughout the entire year with a slightly deeper appearance during winter (Bell and Geller, 2008). Generally, the smallest values of static stability above the thermal tropopause are evident in the region of the subtropical jet (Grise et al., 2010).

In several studies it was shown that a TIL can form from balanced, adiabatic and frictionless dynamics without explicit contributions from radiation in the extratropics. These idealized model simulations span the range from local to global scales, with studies of the dynamics of upper-level anomalies of potential vorticity (further abbreviated with PV) (Wirth, 2003, 2004), of baroclinic life cycles (Erlar and Wirth, 2011), and of the dynamical response to a forcing of a Held–Suarez test (Held and Suarez,

TIL in baroclinic life cycle experiments

D. Kunkel et al.

Title Page

Abstract

Introduction

Conclusions

References

Tables

Figures



Back

Close

Full Screen / Esc

Printer-friendly Version

Interactive Discussion



TIL in baroclinic life cycle experiments

D. Kunkel et al.

Title Page

Abstract

Introduction

Conclusions

References

Tables

Figures



Back

Close

Full Screen / Esc

Printer-friendly Version

Interactive Discussion



1994) in a dry general circulation model (Son and Polvani, 2007). In the latter case, the TIL forms spontaneously under a wide variety of model parameters, such as horizontal and vertical model resolution. From the analysis of positive and negative PV-anomalies it was found that the sharpening of the tropopause was linked to the convergence of the vertical wind. Particularly, this was related to a cross-frontal circulation (Wirth, 2004). Furthermore, the TIL evolved stronger above anticyclonic than over cyclonic flow (Wirth, 2003). This result was confirmed in studies of adiabatic baroclinic life cycles, in which the TIL became evident after breaking of baroclinic waves (Erlar and Wirth, 2011). Recently, the impact of dissipating inertia-gravity waves was suggested to persistently contribute to the formation and maintenance of the TIL. These waves result from imbalances along the jet and the dissipation may alter the thermal structure through energy dissipation, local heating, and turbulent motions (Kunkel et al., 2014). Moreover, Birner (2010) showed that the vertical structure of the residual circulation contributes to the sharpening of the tropopause by inducing a dipole forcing of static stability around the tropopause. This process was identified to significantly add to the tropopause sharpening during winter in the midlatitudes.

Balanced dynamics alone, however, can not explain all features related to the TIL (Son and Polvani, 2007) and as has been shown by Randel et al. (2007) radiative processes contribute significantly to the TIL. From fixed dynamical radiative transfer calculations it was concluded that water vapor cooling around the tropopause and heating by ozone in the lower and middle stratosphere contribute to a layer of enhanced static stability above the thermal tropopause. Particularly, the water vapor cooling has been identified to be a major process for the summer TIL in polar regions (Randel and Wu, 2010).

Thus, several mechanisms have been identified so far to explain the strength and occurrence of the TIL at all latitudes. Since dry dynamics are not sufficient to fully explain all features of the TIL, processes beyond adiabatic and frictionless dynamics are required to close this gap. Especially in the midlatitude tropopause region, all processes, synoptic-scale and stratospheric dynamics as well as the radiative forcings, need to

TIL in baroclinic life cycle experiments

D. Kunkel et al.

Title Page

Abstract

Introduction

Conclusions

References

Tables

Figures



Back

Close

Full Screen / Esc

Printer-friendly Version

Interactive Discussion



be considered. With this knowledge we can ask the question which of the before mentioned processes is most important to form and maintain the TIL. In this study we aim to address this question in the framework of idealized baroclinic life cycles with a limited area, non-hydrostatic model. We extend the work of Erler and Wirth (2011) and include diabatic and mixing processes, i.e., related to humidity, radiation, or turbulence. These processes can violate material conservation of potential vorticity Q and are further referred to as non-conservative processes in this study. Since we focus on a rather short time scale, we assume that the effect of the stratospheric circulation is rather small and exclude this effect in the interpretation of our results. Thus, we focus mainly on the following questions: (1) How do non-conservative processes, i.e., diabatic and mixing processes, alter the TIL evolution in baroclinic life cycles compared to the well-known evolution in the adiabatic and frictionless case? (2) What is the relative importance of individual processes that contribute to the formation the TIL during different stages of the life cycles?

To answer these questions we structured our analysis as follows. In Sect. 2 we introduce the model setup along with the physical parameterizations and a summary of the conducted simulations. We then present results from two sets of simulations. In Sect. 3 we show results from baroclinic life cycles in which only one individual non-conservative process is turned on separately to address question (1). In a second set of simulations we show results of simulations with a successively increasing number of physical processes to address question (2) (Sect. 4). We summarize our results and give further conclusions in Sect. 5.

2 Model formulation and baroclinic life cycle experiments

2.1 Adiabatic model configuration and initial state

We conducted baroclinic life cycle experiments in an idealized, spherical, midlatitude channel configuration of the non-hydrostatic regional model COSMO (CONsortium for

TIL in baroclinic life cycle experiments

D. Kunkel et al.

Title Page

Abstract

Introduction

Conclusions

References

Tables

Figures



Back

Close

Full Screen / Esc

Printer-friendly Version

Interactive Discussion



Small-scale MOdelling, Steppeler et al., 2003). For the adiabatic model we only used the dynamical core of the model which solves the hydro-thermodynamical equations. Only a fourth order horizontal hyper-diffusion had to be applied to guarantee numerical stability. Physical processes such as microphysics, convection, turbulence, radiation are introduced in more detail further below (see Sect. 2.2). Time integration was performed with a third order, two-time-level Runge–Kutta scheme, in which fast terms, i.e., sound and gravity waves, are stepped forward in time with a smaller time step. We use a fifth order centered finite difference approximation in the horizontal and a third order scheme in the vertical. Passive tracer advection was done with a fourth order Bott Scheme with Strang splitting (Doms, 2011).

We studied baroclinic waves with wavenumber six with a model setup similar to Erler and Wirth (2011) and Kunkel et al. (2014). Our model domain spans over 60° longitude and 70° latitude, from the surface up to a height of 25.0 km and with a grid spacing of 0.4° (~ 44 km) in the horizontal and 110 m in the vertical in the region of the tropopause. Consequently, we obtain an aspect ratio ($\Delta z/\Delta x$) of about $1/400$ which is considered favorable to study the TIL (Birner et al., 2006; Erler and Wirth, 2011). In the uppermost seven kilometer of the model domain Rayleigh damping is applied to avoid reflection of upward propagating signals and there is no orography at the bottom. In meridional direction the boundary conditions are relaxed towards the initial values to avoid reflection of outgoing signals, while periodic boundary conditions are specified in the zonal direction.

For the initial conditions we follow Olson and Colle (2007) and Schemm et al. (2013) with slight adaptations to account for the spherical geometry of our approach. A background state is obtained for three dimensional fields of temperature, T , and pressure, p , from which a thermally balanced wind is calculated as in Erler and Wirth (2011). The initial vertical wind, w , is zero and the background state is baroclinically unstable by construction. However, to allow a fast evolution of the baroclinic wave, this state is superimposed by perturbation fields for p , T , u , and v which result from an inversion of a specified PV anomaly. This circular anomaly is introduced in the middle of the

TIL in baroclinic life cycle experiments

D. Kunkel et al.

Title Page

Abstract

Introduction

Conclusions

References

Tables

Figures



Back

Close

Full Screen / Esc

Printer-friendly Version

Interactive Discussion



domain at the altitude of the tropopause. Slight changes in the initial state allow us to study various types of baroclinic life cycles (for details we refer to Olson and Colle, 2007). However, our focus is on the classical LC1 wave type (Thorncroft et al., 1993), since it produces a stronger TIL in the adiabatic case (Erlar and Wirth, 2011). This type is characterized by a thinning trough which then forms a streamer and later a cut-off cyclone, while the baroclinic wave breaks anti-cyclonically. More details on the development of this wave and the corresponding sharpening of the tropopause type are generally given in Erlar and Wirth (2011) and for this setup especially in Kunkel et al. (2014), where the authors used a higher resolution version of this model. It is noted here that the lower resolution model well reproduces the results of Kunkel et al. (2014). For this reason and because of the vast number of conducted model simulations (see Table 1), we decided to use a coarser grid spacing in our simulations.

Figure 1 shows the initial state in the center of our model domain. The zonal wind u has its maximum velocity between the thermal and dynamical tropopause (here defined as the $Q = 2.0$ pvu contour line, with pvu = potential vorticity units, and $1.0 \text{ pvu} = 1.0 \times 10^{-6} \text{ Km}^2 \text{ kg}^{-1} \text{ s}^{-1}$). The thermal tropopause separates tropospheric ($N^2 < 1.5 \times 10^{-4} \text{ s}^{-2}$) from the stratospheric ($N^2 > 4.0 \times 10^{-4} \text{ s}^{-2}$) background values of static stability. The initial zonally symmetric specific humidity field, depicted with the blue lines, has been constructed such that it is comparable in magnitude and distribution to moisture profiles from re-analysis data. For this it is constructed as follows: a constant surface relative humidity (RH_s) is given which decreases linearly with height everywhere. If not specified otherwise, RH_s is 60% and decreases with a gradient of 10%/2 km. Thus, above 12 km altitude the relative humidity (RH) is zero. The model, however, requires specific humidity q_v as input variable. This quantity is obtained by multiplication of the relative humidity with the saturation specific humidity ($q_{vs} : q_v = \text{RH}/100 \cdot q_{vs}$). The latter quantity is computed from the saturation water vapor, which is computed with the parameterization of Magnus (Murray, 1967). A final constraint is given for the initial distribution of q_v , i.e., that $\min(q_v) = 2.0 \times 10^{-6} \text{ kg kg}^{-1}$.

Note that this leads to a constant initial value of $q_v = 2.0 \times 10^{-6} \text{ kg kg}^{-1}$ in the stratosphere in our simulations.

We further use passive tracers to diagnose particular features of our baroclinic life cycles. These tracers are purely advected and not explicitly mixed vertically or horizontally by a parameterization scheme. However, mixing due to numerical reasons does still affect the tracer distribution. In particular, we use three tracers which carry information of the initial state of the baroclinic life cycles: (1) the initial height of each grid box z_0 , (2) the initial static stability N_0^2 , and (3) the initial potential vorticity Q_0 . With these tracers it is possible to calculate the differences between the current and the initial distribution of these quantities and as such obtain information about whether an air parcel has gained or lost (1) altitude, measured by $\Delta z = z - z_0$, (2) static stability, measured by $\Delta N^2 = N^2 - N_0^2$, and (3) changed their potential vorticity because of non-conservative processes, measured by $\Delta Q = Q - Q_0$, with $Q = \rho^{-1} \boldsymbol{\eta} \cdot \nabla \Theta$ and ρ air density, $\boldsymbol{\eta}$ absolute vorticity, and Θ potential temperature.

2.2 Formulation of non-conservative processes in COSMO

2.2.1 Turbulence

Turbulence is calculated for the three dimensional wind (u , v , and w), the liquid water potential temperature (Θ_l), and the total water (q_w) which is the sum of specific water vapor q_v and specific cloud water q_c . Budget equations for the second order moments are reduced under application of a closure of level 2.5 (in the notation of Mellor and Yamada, 1982), i.e., local equilibrium is assumed for all moments except for turbulent kinetic energy (TKE), for which advection and turbulent transport is retained. Three dimensional turbulent effects are neglected which is a valid approximation for simulations on the mesoscale, which means that horizontal homogeneity is assumed. Hence, only vertical turbulent fluxes are parameterized under consideration of the Boussinesq approximation. Moreover, the TKE budget equation depends significantly on the vertical

Title Page

Abstract

Introduction

Conclusions

References

Tables

Figures

◀

▶

◀

▶

Back

Close

Full Screen / Esc

Printer-friendly Version

Interactive Discussion



shear of the horizontal wind components and the vertical change in Θ_1 and q_w . More details are given in Doms (2011).

2.2.2 Cloud microphysics

Cloud microphysics follow a bulk approach using a single moment scheme with five types of water categories being treated prognostically: specific humidity q_v for the gas phase, two non-precipitating cloud types, i.e., cloud water q_c and cloud ice q_i , as well as two precipitating types, i.e., rain q_r and snow q_s . These five water types can interact within various processes such as cloud condensation and evaporation, depositional growth and sublimation of snow, evaporation of snow and rain, melting of snow and cloud ice, homogeneous and heterogeneous nucleation of cloud ice, autoconversion, collection and freezing. More details are given in Doms (2011) and Joos and Wernli (2012).

2.2.3 Radiation

Radiation is parameterized by the δ -2 stream approximation, i.e., separate treatment of solar and terrestrial wavelengths. In total, eight spectral bands are considered, five in the solar range and three infrared bands. Absorbing and scattering gases are water vapor (H_2O) with a variable content as well as CO_2 , O_3 , CH_4 , N_2O , and O_2 with fixed amounts. Aerosols have been totally neglected whereas a cloud radiative feedback can be calculated in all spectral bands. Further details about the general scheme are given in Ritter and Geleyn (1992) and about the implementation in Doms (2011).

2.2.4 Convection

The scheme of Tiedtke (1989) is used to parameterize sub-grid scale convective clouds and their effects on the large scale environment. This approach uses moisture convergence in the boundary layer to estimate the cloud base mass-flux. The convection

TIL in baroclinic life cycle experiments

D. Kunkel et al.

Title Page

Abstract

Introduction

Conclusions

References

Tables

Figures



Back

Close

Full Screen / Esc

Printer-friendly Version

Interactive Discussion



scheme then affects the large-scale budgets of the environmental dry static energy, the specific humidity, and the potential energy.

2.2.5 Surface fluxes

Instead of using a bottom free-slip boundary condition surface fluxes of momentum and heat are calculated explicitly in one experiment. This results in non-zero turbulent transfer coefficients of momentum and heat and thus affects the roughness length and the fluxes of latent and sensible heat. As we will show later, this has some significant effects on the initiation of convection.

2.3 Simulations of baroclinic life cycles

In total we present the results of 17 different simulations of baroclinic life cycles (see Table 1). Variations between the individual simulations are introduced by either the kind or the number of non-conservative processes. Moreover, additional variability is created by changing the initial humidity as well as by the complexity of treating cloud related processes.

In a first set of simulations, we conducted four different baroclinic life cycles. Using the adiabatic and frictionless life cycle as conservative reference simulation (REF), we obtain further results from life cycles additionally including either turbulence, further denoted as TURB, or radiation, RAD, or bulk microphysics, BMP. For these simulations we apply the standard physical parameterizations of COSMO, which were briefly described in the previous section.

We performed further sensitivity simulations for BMP and RAD to test for the impact of initial conditions as well as the model formulation of a diabatic process. For microphysics we conducted in total four additional life cycle experiments. We first tested for the initial specific humidity q_v . In one case we reduced the initial q_v by setting the surface relative humidity to 30% and the gradient to 5.0%/2 km (BMP R30), while we increased the initial q_v by using $RH_s = 80\%$ and a gradient of 13.33%/2 km in another

TIL in baroclinic life cycle experiments

D. Kunkel et al.

Title Page

Abstract

Introduction

Conclusions

References

Tables

Figures



Back

Close

Full Screen / Esc

Printer-friendly Version

Interactive Discussion



TIL in baroclinic life cycle experiments

D. Kunkel et al.

Title Page

Abstract

Introduction

Conclusions

References

Tables

Figures



Back

Close

Full Screen / Esc

Printer-friendly Version

Interactive Discussion



case (BMP R80). Furthermore, we conducted simulations in which we used different schemes to represent cloud processes. In one simulation only warm phase clouds are considered, excluding cloud ice (BMP NOICE). In another simulation condensation and evaporation between water vapor and cloud water is realized by a saturation adjustment process. Since this simulation includes only large scale diabatic effects from latent heating, it has the least additional effects compared to the dry reference (Schemm et al., 2013). Thus, we refer to this case as quasi-adiabatic case (QADI).

In case of radiation we performed sensitivity simulations with respect to the initial distribution of specific humidity and ozone. These two trace gases are thought to have the largest impact on the thermal structure around the tropopause (e.g., Randel et al., 2007; Riese et al., 2012). We conducted one simulation with reduced initial specific humidity (RAD R30), similar to BMP R30, while we explicitly set the specific humidity to zero above the tropopause in another simulation (RAD woSW). In another case we reduced the amount of ozone (RAD rO3). However, we explicitly note here that ozone is poorly represented in the model. Instead of a three dimensional distribution, only a simple vertical distribution is assumed which has a maximum concentration at altitudes which are close to our model top at a pressure of 42 hPa and a total vertically integrated ozone partial pressure of 0.06 Pa. These two parameters are used in the radiation code to calculate the feedback of the solar and thermal extinction by ozone. We reduced the total amount of ozone by one third to estimate whether this has an impact on the strength of the TIL.

In a next step we use a set of simulations with combinations of non-conservative processes to study potential additive effects as well as to assess the relative contribution of individual processes on the TIL formation and maintenance during different stages of the life cycles. For this we compare results from BMP (here as a reference) to results from simulations where we first add radiation (BMP RAD) and turbulence (BMP TURB) individually and then together (BMP RAD TURB). In further simulations we include convective clouds (BMP RAD TURB CONV) and surface fluxes (BMP RAD TURB CONV SURF). The convective activity is much stronger in the simulation with

surface fluxes than in the simulation with the free-slip boundary condition. Hence, BMP RAD TURB CONV SURF can be regarded as simulation with strong convection, while BMP RAD TURB CONV can rather be seen as life cycle with weak to moderate convective activity. A final sensitivity study was conducted in which the cloud radiative forcing has been neglected to study the effect of this feedback in the region of the tropopause (BMP RAD NOCRF).

3 Non-conservative processes and the formation of a TIL in baroclinic life cycles

In a first step we aim to answer the question which non-conservative process, i.e., related to clouds, radiation, or turbulent mixing has the largest impact on the formation of the TIL in baroclinic life cycles. For this we compare first the results of four life cycles, BMP, RAD), vertical turbulence TURB, and REF, before we discuss the effects of initial conditions and process formulations on the model results.

3.1 Impact of non-conservative processes on the TIL evolution

The baroclinic life cycle 1, also known as LC1, has been discussed under various aspects (e.g., Thorncroft et al., 1993) and also in light of the evolution of the tropopause inversion layer (Erlar and Wirth, 2011). Our REF simulation features the same general characteristics of this life cycle and is described in more detail in Kunkel et al. (2014). One dominant feature of the LC1 is the thinning trough, the so-called stratospheric streamer (often also referred to as Θ - or PV-streamer, e.g., Sprenger et al., 2003). In the mature stage of baroclinic wave this feature is evident for instance in the distribution of potential temperature Θ on an isosurface of potential vorticity, e.g., $Q = 2.0$ pvu. The distribution of potential temperature for our four cases is shown in the upper row of Fig. 2. After 120 h of model integration we see similar structures for REF, TURB, and RAD with minor differences in the exact location of the streamer and the absolute

TIL in baroclinic life cycle experiments

D. Kunkel et al.

Title Page

Abstract

Introduction

Conclusions

References

Tables

Figures



Back

Close

Full Screen / Esc

Printer-friendly Version

Interactive Discussion



TIL in baroclinic life cycle experiments

D. Kunkel et al.

Title Page

Abstract

Introduction

Conclusions

References

Tables

Figures



Back

Close

Full Screen / Esc

Printer-friendly Version

Interactive Discussion



values of Θ in the warm sector (red colors). The most complex distribution occurs in BMP with higher temperatures than in the other three simulations at the southern tip of the streamer. These warmer temperatures are associated with cloud processes and the release of latent heat during rapid ascent. Moreover, the entire Θ -field shows a more in-homogeneous appearance compared to the other three simulations.

Our main focus is, however, on the static stability N^2 in the lowermost stratosphere. In particular, we are interested in the regions where the stability increases significantly during the life cycle. This is typically the case within the first kilometer above the thermal tropopause. However, the spatial appearance is not homogeneous, as is evident from the lower panels in Fig. 2. These panels depict the vertical mean of N^2 over the first kilometer above the thermal tropopause. In all four cases large values of N^2 appear in the warm sector west of the streamer, which is in the region of anti-cyclonic flow. This region has been shown to exhibit a stronger TIL in models (Erler and Wirth, 2011; Wirth, 2003) and in observations (Randel et al., 2007). The life cycle with turbulence shows the lowest values of N^2 , while the static stability has generally larger values in the case of radiation than in the reference simulation. In the life cycle with cloud processes we additionally see enhanced values of N^2 on smaller scales than in the other cases. As we will show later these enhancements are related to moist dynamics and vertical motions.

The moist life cycle shows the strongest development in terms of minimum surface pressure, p_s , evolution, in contrast to the life cycle with radiation (Fig. 3a). While all other life cycles show still a deepening of p_s , the absolute minimum pressure has already been reached in BMP after 140 h of model integration. Moreover, by considering two metrics to trace the evolution of the TIL in our life cycles, we infer that the TIL formation differs most significantly from the dry reference case in the moist life cycle. The maximum static stability N_{\max}^2 increases rather spontaneously in BMP instead of more gradually as in the other three simulations (Fig. 3b). After reaching its absolute maximum value, N_{\max}^2 keeps values above $7.0 \times 10^{-4} \text{ s}^{-2}$ at consecutive times. Only after about 130 h after model start N_{\max}^2 in RAD than in REF and TURB has reached the

TIL in baroclinic life cycle experiments

D. Kunkel et al.

Title Page

Abstract

Introduction

Conclusions

References

Tables

Figures



Back

Close

Full Screen / Esc

Printer-friendly Version

Interactive Discussion



same magnitude as in the moist simulation. Furthermore, an earlier increase of N_{\max}^2 is evident in RAD than in REF and TURB, while in the latter case N_{\max}^2 is smaller than in the reference case at all times. A similar picture is obtained from the metric that is used as a proxy for the spatial extent of the TIL in the life cycles, i.e., the area in which $N^2 > 5.5 \times 10^{-4} \text{ s}^{-2}$, denoted as $A_{5.5}$ (Fig. 3c). The earliest appearance is evident in BMP, the latest in TURB. Moreover, the temporal evolution of $A_{5.5}$ clearly shows that the TIL covers a larger area when diabatic processes are included in the life cycles.

So far, we provided a rather descriptive view on the TIL evolution in our life cycles without giving details about the underlying processes. For the case with turbulence the TIL appears weaker due to the tendency of turbulence to reduce strong vertical gradients. Turbulence acts against the effects of dry dynamics which enhance the lower stratospheric stability during the life cycle. Consequently, only a weak TIL forms in this case.

Including radiation results in a stronger TIL than in the reference case. This is related to the radiative feedback of water vapor, which increases over time in the region of the tropopause (Fig. 4a). Since no microphysics is included in RAD, water vapor is transported as a passive tracer in this simulation. Upward motions in the troposphere and tropopause dynamics lead to more water vapor at the altitude of the tropopause, finally changing the water vapor gradient significantly (Fig. 4b). This causes differential cooling by water vapor in the UTLS, which then results in a non-uniform change of the thermal structure (e.g., Zierl and Wirth, 1997). Additionally, recently lifted, moist air is then partly located also in the lower stratosphere, where its residence time is longer and thus can potentially affect the thermal structure over longer time scales. This process further enhances the static stability directly above the tropopause and thus strengthens the TIL which also forms by the dynamics of the baroclinic wave. Thus, a process directly changing the thermal structure alters the appearance of the TIL in the case with radiation.

In the moist case we present evidence that a process at lower tropospheric levels is responsible for the different appearance of the TIL. The spontaneous increase in

TIL in baroclinic life cycle experiments

D. Kunkel et al.

Title Page

Abstract

Introduction

Conclusions

References

Tables

Figures



Back

Close

Full Screen / Esc

Printer-friendly Version

Interactive Discussion



N_{\max}^2 is well correlated with the earliest release of latent heat in the model (Fig. 5a and b). Since the same effect is evident from the simulation with the saturation adjustment scheme (QADI), we can conclude that it is the release of latent heat rather than a microphysical process being responsible for the observed effect. Latent heat release is, however, not only a sign of condensation but also fosters vertical motions in the model. These vertical motions reach in many cases the tropopause and often lift this vertical transport barrier. Consequently, also the air above is slightly lifted which increases the convergence of isentropic surfaces and thus enhances the static stability above the tropopause. This process differs, however, fundamentally from the process related to dry dynamics on spatial and temporal scales. While the latter is rather slow and occurs predominantly in an anti-cyclonic flow region with on average descending air motion, this lifting process is fast, occurs on small scales, and is related to upward motions. Thus taken together, the incorporation of water in the model fosters a stronger TIL development as consequence of enhanced upward motions within the life cycle due to the release of latent heat. The relation between moisture and vertical motions in moist baroclinic life cycles has also been discussed by Gutowski et al. (1992).

Although the temporal and spatial appearance of the TIL is rather heterogeneous in all four simulations, the TIL becomes also evident in the domain mean vertical profiles of N^2 . These averages are obtained between 25° – 65° N in the meridional direction and in the entire zonal direction. ΔN^2 represents the difference between the current N^2 and the passively advected tracer N_0^2 (Fig. 6a) and ΔQ the difference between the current potential vorticity Q and the passively advected initial potential vorticity Q_0 (Fig. 6b), respectively. The vertical profiles of ΔN^2 and ΔQ are given in a tropopause based coordinate system for every 24 h of the model integration and the thin solid line shows the location of the tropopause. In all four simulations an increase in static stability forms sooner or later during the life cycles just above the tropopause. While the domain mean TIL appears only during the late stages in REF and TURB, it is much earlier obvious in RAD and BMP. However, PV at the tropopause shows significant positive changes only in the simulation with radiation. In contrast, only minor changes of PV are found in the

simulations with turbulence and cloud processes. In the latter case the largest changes of PV occur rather at low- and mid-tropospheric altitudes where the major release of latent heat occurs. In the reference case the minor changes of potential vorticity are solely related to the numerics, especially to the tracer advection scheme (Kunkel et al., 2014). Thus, in case of radiation the formation of the TIL is directly related to a diabatic process in the tropopause region, while the diabatic processes related to clouds have an indirect impact on the TIL, i.e., the diabatic processes and the response of the static stability above the tropopause occur at a different places. Mixing, like radiation, also directly affects the TIL but to a much lesser extent.

3.2 Sensitivity of individual diabatic processes

In the next paragraphs we briefly discuss the impact of initial conditions on the model results, focusing especially on experiments with cloud microphysics and radiation.

For microphysics we tested for the amount of initial specific humidity, comparing BMP to BMP R30, and BMP R80, as well as for the representation of the cloud processes, comparing BMP to BMP NOICE, and QADI. From the temporal evolution of N_{\max}^2 (Fig. 7a) we infer that the amount of specific humidity is more important than the model formulation of cloud processes. If more water is initially present, then the TIL appears earlier. In contrast, with less initial water the TIL appears later and approximates towards the adiabatic case. Moreover, the occurrence of the TIL is relatively insensitive to the representation of the cloud processes as long as the initial amount of specific humidity is the same as it is the case in BMP, BMP NOICE, and QADI.

In case of radiation we tested for the initial amount and distribution of water, comparing RAD to RAD R30, and RAD woSW, as well as for the amount of ozone, comparing RAD to RAD rO3. We find only minor differences in the evolution of N_{\max}^2 for the various sensitivity simulations (Fig. 7b). Reducing the amount of water leads to a reduced radiative feedback and thus to a less strong TIL. Changing the amount of ozone has, in our case, no significant effect at all, however, with the caveat of the simple representation of ozone in our model. The largest difference is found if we completely

Title Page

Abstract

Introduction

Conclusions

References

Tables

Figures



Back

Close

Full Screen / Esc

Printer-friendly Version

Interactive Discussion



remove the water in the stratosphere. This results in an artificially high water vapor gradient between the troposphere and the stratosphere. As we have seen before (Fig. 4), a strong water vapor gradient results in a sharp tropopause. A similar result has been discussed by Fusina and Spichtinger (2010) who studied amongst many other features the response of the static stability to the sharpness of a gradient between saturated and unsaturated air.

4 Relative importance of dynamical and diabatic processes on the TIL formation

Until here we provided new insights of the isolated effect of individual physical processes on the formation of the tropopause inversion layer in baroclinic life cycles. Now we turn our discussion to relative importance of these processes, and especially whether the dynamical or the radiative forcing is more important for the TIL formation and maintenance. For this purpose we use our second set of baroclinic life cycle experiments where we successively increase the number of processes and as such increase complexity. The simulation with cloud processes (BMP) serves as reference while we first add radiation (BMP RAD) and turbulence (BMP TURB) separately and then combine all three processes (BMP RAD TURB). We further add convection (BMP RAD TURB CONV) and then also surface fluxes of momentum and heat (BMP RAD TURB CONV SURF).

The six life cycles evolve similar, all forming a Θ -streamer and anti-cyclonic wave breaking. Again the temperature distribution at the southern tip of the streamer varies most between the individual life cycles (Fig. 8). Moreover, in some cases a smooth Θ -distribution is evident, e.g., BMP TURB, BMP TURB RAD, or BMP TURB RAD CONV, while the distribution is more variable and shows more small scale features in other life cycles, especially in BMP RAD TURB CONV SURF. The static stability above the tropopause has its largest values in the anti-cyclonic part of the wave where often two maxima are evident. The first maximum occurs along the cold front ahead of the

TIL in baroclinic life cycle experiments

D. Kunkel et al.

Title Page

Abstract

Introduction

Conclusions

References

Tables

Figures



Back

Close

Full Screen / Esc

Printer-friendly Version

Interactive Discussion



TIL in baroclinic life cycle experiments

D. Kunkel et al.

Title Page

Abstract

Introduction

Conclusions

References

Tables

Figures



Back

Close

Full Screen / Esc

Printer-friendly Version

Interactive Discussion



cyclonic center where the warm conveyor belt (WCB) lifts moist air masses into the tropopause region. Such a relation between WCB and TIL has been proposed by Peevey et al. (2014) who used HIRDLS satellite and ECMWF model data to obtain their results. The other maximum is located more at the western side of the streamer where inertia-gravity waves are generated and influence the thermal structure of the tropopause (Kunkel et al., 2014). In case of BMP RAD TURB CONV SURF a larger area exhibits enhanced static stability values above the tropopause which is the result of convective activity as we will see later in more detail.

In the following we aim to answer the question why the TIL appears earlier in some life cycles and how the TIL is maintained after it has been generated. We first compare the time of first appearance of the TIL between the six life cycles. Figure 9a–e shows the first 80 h of model integration for various variables. The initial increase of N_{\max}^2 can be divided into three sections which are related to the physical processes considered in the respective life cycle (Fig. 9a). The latest TIL appearance after about 65 h is found when considering only cloud processes and turbulence. Including radiation to the model simulations shifts the time of appearance ten hours ahead, while the earliest TIL formation starts already after about 35 h in case of considering convection and surface fluxes. This division into three time sectors correlates well with a proxy for strong updrafts, for which we use the tracer which carries the initial height information of an air parcel. With this information we can calculate the difference Δz which is positive if an air parcel raised and is negative if air parcel descended since model start. Figure 9b depicts the maximum Δz in the layer between the thermal tropopause and 500 m below this level, from which we infer that there is strong temporal coincidence between the first appearance of N_{\max}^2 and updrafts originating at low levels. The earlier appearance of updrafts in case with radiation and convection is related to the these processes, since they foster an earlier emerging of conditional instability. This finding supports our results from the previous section that moist dynamics including strong updrafts has a strong impact on the first appearance of the TIL. These updrafts further enhance the local convergence of the vertical wind just above the tropopause as

TIL in baroclinic life cycle experiments

D. Kunkel et al.

Title Page

Abstract

Introduction

Conclusions

References

Tables

Figures



Back

Close

Full Screen / Esc

Printer-friendly Version

Interactive Discussion



we will see later. Moreover, we find good agreement between the temporal increase of N_{\max}^2 and two tracers for moisture, specific humidity q_v (Fig. 9c) and specific cloud ice content q_i (Fig. 9d). Thus, the updrafts moisten the upper troposphere below the tropopause which, as shown before, supports the TIL formation by radiative cooling.

The gradual increase of N_{\max}^2 in case of BMP RAD TURB CONV SURF can further be related to another tracer for updrafts, which is the cloud base mass flux which is available for the two simulations in which the convective cloud parameterization is switched on (Fig. 9e). This quantity serves as proxy for convective activity and starts to increase gradually in the case with surface fluxes early during the simulation. Thus, these findings further support our suggestion from Sect. 3 that vertical motions are the essential key parameter for the initial TIL appearance in baroclinic life cycles with diabatic and mixing processes.

We further provide evidence that there is not only a temporal but also a spatial coincidence between updrafts and TIL occurrence. Figure 10 shows zonal cross-sections of N^2 for the six simulations along 45° N after 144 h of model integration. Indications of increased static stability are found in all cases above the updrafts which reach the tropopause. Clouds often form in the regions of the updrafts and in the lowermost stratosphere we find regions of convergence of the vertical wind. This convergence results from emerging gravity waves from the updrafts, but is also present in regions of propagating inertia-gravity in the eastern most region of the cross-sections. Gravity waves can alter the TIL temporarily during propagation (Otsuka et al., 2014) and possibly permanently by breaking or wave capture (Kunkel et al., 2014). In addition to the effects of dry dynamics, i.e., distribution of cyclonic and anti-cyclonic flow and breaking of the baroclinic wave (see Erler and Wirth, 2011), the effects from updrafts, small-scale convergence, and radiation, contribute most strongly to the TIL formation. Furthermore, note that low-, and mid-tropospheric diabatic heating causes a negative change in PV above the region of maximum heating, thus enhancing the anti-cyclonic flow in the tropopause region above (e.g., Joos and Wernli, 2012), which further has a positive feedback on the TIL evolution.

TIL in baroclinic life cycle experiments

D. Kunkel et al.

Title Page

Abstract

Introduction

Conclusions

References

Tables

Figures



Back

Close

Full Screen / Esc

Printer-friendly Version

Interactive Discussion



To this point we showed that updrafts are initially important to form the TIL. However, this contribution seems to decrease over time. To support this hypothesis we calculated the difference between the mean of static stability in regions of strong updrafts N_{dz}^2 , i.e., where $\Delta z \geq 2.5$ km, and the domain mean N^2 , denoted as $N_{dz}^2 - N^2$ (see Fig. 11). We did this every 24 h of model integration and use a tropopause based coordinate system. From this we conclude that the difference $N_{dz}^2 - N^2$ becomes generally smaller over time which is partly attributable to the domain mean TIL which becomes stronger but also to the fact that the number of model grid cells in which $\Delta z \geq 2.5$ km does not significantly grow during the last days (see numbers in the top left corners). We did the same analysis for convergent regions, with a threshold of $\partial w / \partial z \leq 5.0 \times 10^{-5} \text{ s}^{-1}$ and calculated the mean profile N_{wz}^2 . The difference $N_{wz}^2 - N^2$ becomes smaller with integration time but also the region which contributes to N_{wz}^2 increases, especially at times when vertical motions rather tend to have a smaller impact. Only in the case with surface fluxes the convective updrafts dominate over the entire life cycle. Nevertheless, we can conclude that convergence of the vertical wind is important in forming and maintaining the TIL. However, the process leading to the convergence may differ with time during the life cycle. While updrafts are more important during the period of first TIL occurrence, propagating (inertia-) gravity waves become more important at later times.

We already saw that moistening the upper troposphere fosters the evolution of the TIL. Since ice clouds also reach the level of the tropopause, we briefly discuss their potential impact on the thermal structure above the tropopause. We only use cloud processes and radiation in this analysis here and exclude the effects of mixing and convection. We conducted a further simulation in which we turned off the cloud radiative feedback feedback (BMP RAD NOCRF) and compare the results to those from a simulation with feedback (BMP RAD) to assess the impact of ice clouds on TIL in the model. From instantaneous vertical profiles of meteorological and tracer quantities within regions which exhibit a TIL and ice clouds up to the tropopause we infer the following points (Fig. 12): (1) the net heating rate is much more negative in the upper

TIL in baroclinic life cycle experiments

D. Kunkel et al.

Title Page

Abstract

Introduction

Conclusions

References

Tables

Figures



Back

Close

Full Screen / Esc

Printer-friendly Version

Interactive Discussion



5 troposphere when the forcing is turned on, with the cooling being strongest just below the thermal tropopause (black solid lines); (2) the temperature profile in the UTLS differs significantly between both cases – while there is a clear minimum in the case with cloud radiative forcing, an almost neutral temperature profile is evident in the first
10 two kilometers above the tropopause in BMP RAD NOCRF (black dashed lines); (3) the upper edge of the ice cloud is located slightly above the tropopause in BMP RAD and slightly below in the other case (blue solid lines); (4) the specific humidity has a local maximum at the top of the ice cloud which is stronger in the case with feedback (blue dashed lines); (5) the static stability is increased in both cases with a slightly
15 higher located and stronger maximum in case with feedback (red solid lines); (6) the height tracer indicates lifted air mass in the troposphere below the maximum of static stability, however, with stronger updrafts in the case with feedback (red dashed lines). From points (1), (2), and (5) we conclude that the tropopause can be sharper due to strong differential cooling in the UTLS, if ice clouds are present. Moreover, from (3), (4), and (6) it follows that the potential to moisten the lower stratosphere is also increased
20 which might in turn enhance the radiative formation process of the TIL. Thus, the results from this sensitivity suggest that there is a larger potential to obtain a stronger TIL when clouds reach up to the level of the tropopause. Moreover, this might be of further interest, since ice clouds, or ice super-saturated regions, have been shown to occur frequently in the lower stratosphere (e.g., Spichtinger et al., 2003; Spang et al., 2015).

25 So far we mainly focused on diabatic effects. In the last paragraph we turn to the effect of mixing and analyze where turbulent mixing occurs at the tropopause and whether this spatially and temporally coincides with the appearance of the TIL. Turbulent mixing contributes to the process of small scale stratosphere-troposphere exchange (STE). It has been speculated in several studies that TIL and STE are causally related beyond a pure spatial coincidence (e.g., Gettelman and Wang, 2015). Kunkel et al. (2009) used airborne measurements and ECMWF analysis data from which they concluded that mixing at the tropopause is a synoptic scale process on rather short time scales which, however, enhances the concentration of radiatively active trace

TIL in baroclinic life cycle experiments

D. Kunkel et al.

[Title Page](#)[Abstract](#)[Introduction](#)[Conclusions](#)[References](#)[Tables](#)[Figures](#)[Back](#)[Close](#)[Full Screen / Esc](#)[Printer-friendly Version](#)[Interactive Discussion](#)

gases in the mixing layer. This then leads to an increase in static stability further downwind of the region of the STE event. Thus, they focused on the long term relation between mixing and N^2 . On the other hand we see that values of turbulent kinetic energy (TKE) are often increased in regions where a TIL is present (Fig. 13). These values are smaller than in the boundary layer, but nevertheless increased compared to the background values in the tropopause region at other locations and times in our model simulations. Such exchange events may have only spatial extension of a few tenths of kilometers or even less. Müller et al. (2015) recently reported a comparable event based on airborne in-situ measurements of nitrous oxide, ozone, and ice cloud particles. However, since our model is not capable of resolving this process with sufficient accuracy to conduct a quantitative estimate of STE, we will leave a more detailed analysis open to further studies.

5 Conclusions and summary

By conducting various simulations of baroclinic life cycles we aimed to improve the understanding whether dynamical or diabatic processes are more relevant to form a tropopause inversion layer (TIL). For this we used the non-hydrostatic, limited area model COSMO in a midlatitude channel configuration along with a varying number of physical parameterizations. We first analyzed the effect of individual diabatic processes, i.e., related to clouds and radiation, and mixing processes before we estimated the relative importance of each process.

In a first set of simulations the evolution of the TIL has been compared in baroclinic life cycles. A life cycle with only dry dynamics served as reference, while in three more life cycles one additional non-conservative processes. We further assessed the impact of initial conditions and process formulation in the diabatic cases. In a second step we successively increased the number of processes to assess the relative importance of the various dynamical and diabatic processes to the TIL evolution.

Most importantly, our experiments highlighted the role of different moisture related processes for the formation and evolution of the TIL with varying relevance and strength in different phases of the baroclinic life cycles. In detail, we derived the following results:

1. A TIL forms in baroclinic life cycles with only dry dynamics as well as in life cycles with additionally either vertical turbulence, cloud processes, or radiation. Compared to the dry reference case the TIL appears weaker with respect to its maximum value as well as to the spatial appearance in the case with turbulence. The opposite is evident in the case with radiation with a larger maximum static stability and larger spatial appearance. The temporal evolution is, however, still similar to the reference case. This is different with cloud processes. The TIL emerges much earlier and shows generally the largest maximum values and spatial extension.
2. The processes forming the TIL in the cases with diabatic and mixing processes are as follows. Turbulence acts against the forming process from dynamics, i.e., sharpening the lower stratosphere, and as such a weaker TIL is the final result. With only radiative processes, the (passive) transport of moisture from low to high levels leads to an increase in the moisture burden in the UTLS and to a change in the moisture gradient in this region. The UTLS is then cooled non-uniformly which finally further enhances the static stability above the tropopause. The important process with clouds is the release of latent heat during condensation. This increases the frequency and strength of vertical motions which locally increase the static stability above the regions of the updrafts. Especially, the TIL forms in the region of the warm conveyor belt. In contrast to the direct diabatic forcing (occurring in the region of the tropopause) in the case with radiation, the enhancement of static stability results from a diabatic forcing at lower levels in the case with clouds.
3. Analysis of initial conditions and process formulations showed that the TIL formation in the model is relative insensitive to the formulation of the cloud forming process itself and more dependent on the initial amount of specific humidity. For

TIL in baroclinic life cycle experiments

D. Kunkel et al.

Title Page

Abstract Introduction

Conclusions References

Tables Figures

◀ ▶

◀ ▶

Back Close

Full Screen / Esc

Printer-friendly Version

Interactive Discussion



radiation no significant dependency on the initial water or ozone amount is evident. Here, the change of the gradient of specific humidity is the more important process.

4. Further simulations of baroclinic life cycles with varying complexity with respect to the number of incorporated physical processes showed that there is a correlation between the first appearance of the TIL and of updrafts reaching the tropopause. However, the exact timing of this first occurrence further depends on the included physical processes. The TIL emerges latest when only cloud processes and turbulence are considered while it appears earlier when radiation is incorporated and even more with convection. From this result it is concluded that updrafts are the key process in the initial formation of the TIL in moist baroclinic life cycles, however, noting that their effect is probably fading with time.
5. The updrafts that reach the tropopause lead to the emission of gravity wave in the lower stratosphere. Such small scale waves have a further source in the jet-front system (inertia-gravity waves). It has been shown that these small-scale disturbances can alter the thermal structure above the tropopause temporarily as well as permanently and as such affect the TIL during the entire life cycle after their first appearance.
6. Finally, updrafts enhance the moisture content of the upper troposphere, not only by transporting water vapor to this altitude. Clouds also form within the updrafts. These clouds locally influence the thermal structure of the upper troposphere such that there is a larger potential to obtain a stronger TIL. Generally, the radiative impacts become more relevant during later stages of the life cycle.

Thus, the various dynamical and diabatic processes lead to a highly variable temporal and spatial appearance of the TIL on the time-scale of a week. In reality the TIL in the midlatitudes may be restrengthened by each passing baroclinic wave and the lifted water vapor serves as a cooling agent in the upper troposphere and even in

TIL in baroclinic life cycle experiments

D. Kunkel et al.

Title Page

Abstract

Introduction

Conclusions

References

Tables

Figures



Back

Close

Full Screen / Esc

Printer-friendly Version

Interactive Discussion



the lower stratosphere over a longer time-scale than a week. Including the frequency of occurrence of baroclinic waves might further help to explain the quasi-permanent appearance of a layer of enhanced static stability.

Acknowledgements. D. Kunkel acknowledges funding from the German Science Foundation under grant HO 4225/2-1. The authors thank A. Roches, U. Blahak, and S. Schemm for model support and the HPC team of the university of Mainz for computing time. We further thank P. Spichtinger for valuable comments on an earlier version of the manuscript. Further information on data (model code and output) relevant to this paper can be obtained upon request via email to the authors (dkunkel@uni-mainz.de).

References

- Bell, S. W. and Geller, M. A.: Tropopause inversion layer: seasonal and latitudinal variations and representation in standard radiosonde data and global models, *J. Geophys. Res.-Atmos.*, 113, D05109, doi:10.1029/2007JD009022, 2008. 21497
- Birner, T.: Fine-scale structure of the extratropical tropopause region, *J. Geophys. Res.*, 111, D04104, doi:10.1029/2005JD006301, 2006. 21497
- Birner, T.: Residual Circulation and Tropopause Structure, *J. Atmos. Sci.*, 67, 2582–2600, doi:10.1175/2010JAS3287.1, 2010. 21498
- Birner, T., Dörnbrack, A., and Schumann, U.: How sharp is the tropopause at midlatitudes?, *Geophys. Res. Lett.*, 29, 1700, doi:10.1029/2002GL015142, 2002. 21497
- Birner, T., Sankey, D., and Shepherd, T. G.: The tropopause inversion layer in models and analyses, *Geophys. Res. Lett.*, 33, L14804, doi:10.1029/2006GL026549, 2006. 21497, 21500
- Doms, G.: A Description of the Nonhydrostatic Regional COSMO-Model, Part I: Dynamics and Numerics, Tech. rep., Deutscher Wetterdienst, Offenbach, Germany, 2011. 21500, 21503
- Erlar, A. R. and Wirth, V.: The static stability of the tropopause region in adiabatic baroclinic life cycle experiments, *J. Atmos. Sci.*, 68, 1178–1193, doi:10.1175/2010JAS3694.1, 2011. 21497, 21498, 21499, 21500, 21501, 21506, 21507, 21513
- Fusina, F. and Spichtinger, P.: Cirrus clouds triggered by radiation, a multiscale phenomenon, *Atmos. Chem. Phys.*, 10, 5179–5190, doi:10.5194/acp-10-5179-2010, 2010. 21511

Title Page

Abstract

Introduction

Conclusions

References

Tables

Figures



Back

Close

Full Screen / Esc

Printer-friendly Version

Interactive Discussion



TIL in baroclinic life cycle experiments

D. Kunkel et al.

Title Page

Abstract

Introduction

Conclusions

References

Tables

Figures



Back

Close

Full Screen / Esc

Printer-friendly Version

Interactive Discussion



- Gettelman, A. and Wang, T.: Structural diagnostics of the tropopause inversion layer and its evolution, *J. Geophys. Res.-Atmos.*, 120, 46–62, doi:10.1002/2014JD021846, 2015. 21497, 21515
- Grise, K. M., Thompson, D. W. J., and Birner, T.: A global survey of static stability in the stratosphere and upper troposphere, *J. Climate*, 23, 2275–2292, doi:10.1175/2009JCLI3369.1, 2010. 21497
- Gutowski, W. J., Branscome, L. E., and Stewart, D. A.: Life cycles of moist baroclinic eddies, *J. Atmos. Sci.*, 49, 306–319, doi:10.1175/1520-0469(1992)049<0306:LCOMBE>2.0.CO;2, 1992. 21509
- Held, I. M. and Suarez, M. J.: A proposal for the intercomparison of the dynamical cores of atmospheric general circulation models, *B. Am. Meteorol. Soc.*, 75, 1825–1830, doi:10.1175/1520-0477(1994)075<1825:APFTIO>2.0.CO;2, 1994. 21497
- Joos, H. and Wernli, H.: Influence of microphysical processes on the potential vorticity development in a warm conveyor belt: a case-study with the limited-area model COSMO, *Q. J. Roy. Meteor. Soc.*, 138, 407–418, doi:10.1002/qj.934, 2012. 21503, 21513
- Kunkel, D., Hoor, P., and Wirth, V.: Can inertia-gravity waves persistently alter the tropopause inversion layer?, *Geophys. Res. Lett.*, 41, 7822–7829, doi:10.1002/2014GL061970, 2014. 21498, 21500, 21501, 21506, 21510, 21512, 21513
- Kunz, A., Konopka, P., Müller, R., Pan, L. L., Schiller, C., and Rohrer, F.: High static stability in the mixing layer above the extratropical tropopause, *J. Geophys. Res.*, 114, D16305, doi:10.1029/2009JD011840, 2009. 21515
- Mellor, G. L. and Yamada, T.: Development of a turbulence closure model for geophysical fluid problems, *Rev. Geophys.*, 20, 851, doi:10.1029/RG020i004p00851, 1982. 21502
- Müller, S., Hoor, P., Berkes, F., Bozem, H., Klingebiel, M., Reutter, P., Smit, H. G. J., Wendisch, M., Spichtinger, P., and Borrmann, S.: In situ detection of stratosphere-troposphere exchange of cirrus particles in the midlatitudes, *Geophys. Res. Lett.*, 42, 949–955, doi:10.1002/2014GL062556, 2015. 21516
- Murray, F. W.: On the computation of saturation vapor pressure, *J. Appl. Meteorol.*, 6, 203–204, doi:10.1175/1520-0450(1967)006<0203:OTCOSV>2.0.CO;2, 1967. 21501
- Olson, J. B. and Colle, B.: A modified approach to initialize an idealized extratropical cyclone within a mesoscale model, *Mon. Weather Rev.*, 135, 1614–1624, doi:10.1175/MWR3364.1, 2007. 21500, 21501

TIL in baroclinic life cycle experiments

D. Kunkel et al.

Title Page

Abstract

Introduction

Conclusions

References

Tables

Figures



Back

Close

Full Screen / Esc

Printer-friendly Version

Interactive Discussion



Otsuka, S., Takeshita, M., and Yoden, S.: A numerical experiment on the formation of the tropopause inversion layer associated with an explosive cyclogenesis: possible role of gravity waves, *Progress in Earth and Planetary Science*, 1, 19, doi:10.1186/s40645-014-0019-0, 2014. 21513

5 Peevey, T. R., Gille, J. C., Homeyer, C. R., and Manney, G. L.: The double tropopause and its dynamical relationship to the tropopause inversion layer in storm track regions, *J. Geophys. Res.-Atmos.*, 119, 10194–10212, doi:10.1002/2014JD021808, 2014. 21512

Randel, W. J. and Wu, F.: The Polar summer tropopause inversion layer, *J. Atmos. Sci.*, 67, 2572–2581, doi:10.1175/2010JAS3430.1, 2010. 21497, 21498

10 Randel, W. J., Wu, F., and Forster, P.: The extratropical tropopause inversion layer: global observations with GPS data, and a radiative forcing mechanism, *J. Atmos. Sci.*, 64, 4489–4496, doi:10.1175/2007JAS2412.1, 2007. 21497, 21498, 21505, 21507

Riese, M., Ploeger, F., Rap, A., Vogel, B., Konopka, P., Dameris, M., and Forster, P.: Impact of uncertainties in atmospheric mixing on simulated UTLS composition and related radiative effects, *J. Geophys. Res.*, 117, D16305, doi:10.1029/2012JD017751, 2012. 21505

15 Ritter, B. and Geleyn, J.-F.: A comprehensive radiation scheme for numerical weather prediction models with potential applications in climate simulations, *Mon. Weather Rev.*, 120, 303–325, doi:10.1175/1520-0493(1992)120<0303:ACRSFN>2.0.CO;2, 1992. 21503

Schemm, S., Wernli, H., and Papritz, L.: Warm conveyor belts in idealized moist baroclinic wave simulations, *J. Atmos. Sci.*, 70, 627–652, doi:10.1175/JAS-D-12-0147.1, 2013. 21500, 21505

20 Son, S.-W. and Polvani, L. M.: Dynamical formation of an extra-tropical tropopause inversion layer in a relatively simple general circulation model, *Geophys. Res. Lett.*, 34, L17806, doi:10.1029/2007GL030564, 2007. 21498

25 Spang, R., Günther, G., Riese, M., Hoffmann, L., Müller, R., and Griessbach, S.: Satellite observations of cirrus clouds in the Northern Hemisphere lowermost stratosphere, *Atmos. Chem. Phys.*, 15, 927–950, doi:10.5194/acp-15-927-2015, 2015. 21515

Spichtinger, P., Gierens, K., Leiterer, U., and Dier, H.: Ice supersaturation in the tropopause region over Lindenberg, Germany, *Meteorol. Z.*, 12, 143–156, doi:10.1127/0941-2948/2003/0012-0143, 2003. 21515

30 Sprenger, M., Croci Maspoli, M., and Wernli, H.: Tropopause folds and cross-tropopause exchange: a global investigation based upon ECMWF analyses for the time period March 2000

to February 2001, J. Geophys. Res.-Atmos., 108, 8518, doi:10.1029/2002JD002587, 2003. 21506

5 Steppeler, J., Doms, G., Schättler, U., Bitzer, H. W., Gassmann, A., Damrath, U., and Gregoric, G.: Meso-gamma scale forecasts using the nonhydrostatic model LM, Meteorol. Atmos. Phys., 82, 75–96, doi:10.1007/s00703-001-0592-9, 2003. 21500

Thorncroft, C. D., Hoskins, B. J., and McIntyre, M. E.: Two paradigms of baroclinic-wave life-cycle behaviour, Q. J. Roy. Meteor. Soc., 119, 17–55, doi:10.1002/qj.49711950903, 1993. 21501, 21506

10 Tiedtke, M.: A comprehensive mass flux scheme for cumulus parameterization in large-scale models, Mon. Weather Rev., 117, 1779–1800, doi:10.1175/1520-0493(1989)117<1779:ACMFSF>2.0.CO;2, 1989. 21503

Wirth, V.: Static stability in the extratropical tropopause region, J. Atmos. Sci., 60, 1395–1409, doi:10.1175/1520-0469(2003)060<1395:SSITET>2.0.CO;2, 2003. 21497, 21498, 21507

15 Wirth, V.: A dynamical mechanism for tropopause sharpening, Meteorol. Z., 13, 477–484, 2004. 21497, 21498

Zierl, B. and Wirth, V.: The influence of radiation on tropopause behavior and stratosphere-troposphere exchange in an upper tropospheric anticyclone, J. Geophys. Res., 102, 23883, doi:10.1029/97JD01667, 1997. 21508

TIL in baroclinic life cycle experiments

D. Kunkel et al.

Title Page

Abstract

Introduction

Conclusions

References

Tables

Figures



Back

Close

Full Screen / Esc

Printer-friendly Version

Interactive Discussion



TIL in baroclinic life cycle experiments

D. Kunkel et al.

Title Page

Abstract Introduction

Conclusions References

Tables Figures

◀ ▶

◀ ▶

Back Close

Full Screen / Esc

Printer-friendly Version

Interactive Discussion



Table 1. Summary of experiment acronyms, description, and water treatment

Experiment	Short description	Water species
REF	adiabatic reference simulation	no water species
BMP	standard cloud microphysics	interactive water
RAD	standard radiation scheme	passive water vapor
TURB	standard turbulence scheme	no water species
BMP R30	BMP sensitivity, reduced specific water vapor	interactive water
BMP R80	BMP sensitivity, increased specific water	interactive water
BMP NOICE	BMP sensitivity, only warm clouds	interactive water, no ice phase
QADI	BMP sensitivity, saturation adjustment	water vapor and cloud water
RAD woSW	RAD sensitivity, no stratospheric water	passive water vapor
RAD R30	RAD sensitivity, reduced specific water vapor	passive water vapor
RAD rO3	RAD sensitivity, reduced ozone concentration	passive water vapor
BMP RAD	cloud microphysics and radiation	interactive water
BMP RAD	cloud microphysics and radiation	interactive water
NOCRF	no cloud radiative feedback	
BMP TURB	cloud microphysics and turbulence	interactive water
BMP RAD	cloud microphysics, radiation	interactive water
TURB	and turbulence	
BMP RAD	cloud microphysics, radiation,	interactive water
TURB CONV	turbulence, and convection	
BMP RAD	cloud microphysics, radiation,	interactive water
TURB CONV	turbulence, convection, and surface	
SURF	fluxes for momentum and heat	

TIL in baroclinic life cycle experiments

D. Kunkel et al.

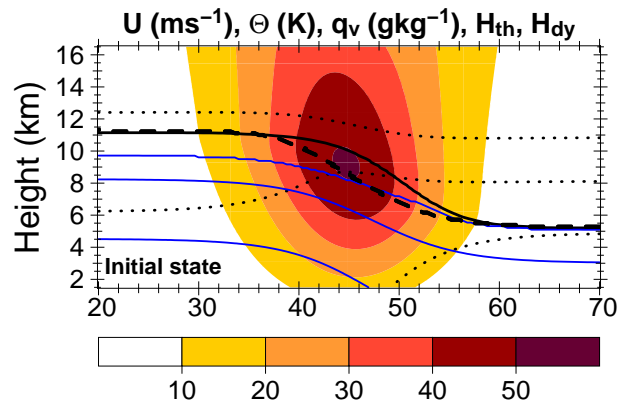


Figure 1. Meridional cross section of the initial state at the center of the model domain: the zonal wind U is color-coded for values of 10, 20, 30, 40, and 50 ms^{-1} ; the potential temperature Θ is shown by the black dotted lines for 280, 320, and 360 K (from bottom to top); the water vapor mixing ratio is shown by the blue lines for values of 2.0, 0.2, and 0.002 gkg^{-1} (from bottom to top); the location of thermal tropopause is indicated by the solid thick black line and separates also the region of tropospheric values ($N^2 < 1.5 \times 10^{-4} \text{ s}^{-2}$) from stratospheric values ($N^2 \sim 4.0 \times 10^{-4} \text{ s}^{-2}$) of static stability; the location of the dynamical tropopause, defined as the isosurface of potential vorticity $Q = 2.0 \text{ pvu}$, is shown by the dashed thick line.

Title Page

Abstract

Introduction

Conclusions

References

Tables

Figures

◀

▶

◀

▶

Back

Close

Full Screen / Esc

Printer-friendly Version

Interactive Discussion



TIL in baroclinic life cycle experiments

D. Kunkel et al.

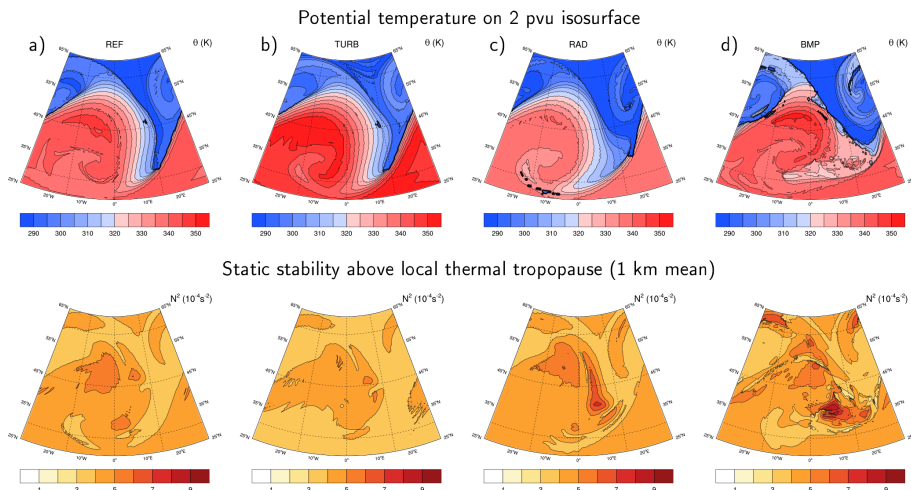


Figure 2. Dynamical and thermodynamical state of the baroclinic life cycles after 120 h of model integration. In the upper row the distribution of Θ (in K) on the dynamical tropopause is depicted, while the lower row shows the distribution of static stability N^2 (in 10^{-4} s^{-2}) averaged over the first kilometer above the thermal tropopause. The four columns show from left to right the following simulations: **(a)** REF, **(b)** TURB, **(c)** RAD, and **(d)** BMP.

Title Page

Abstract

Introduction

Conclusions

References

Tables

Figures



Back

Close

Full Screen / Esc

Printer-friendly Version

Interactive Discussion



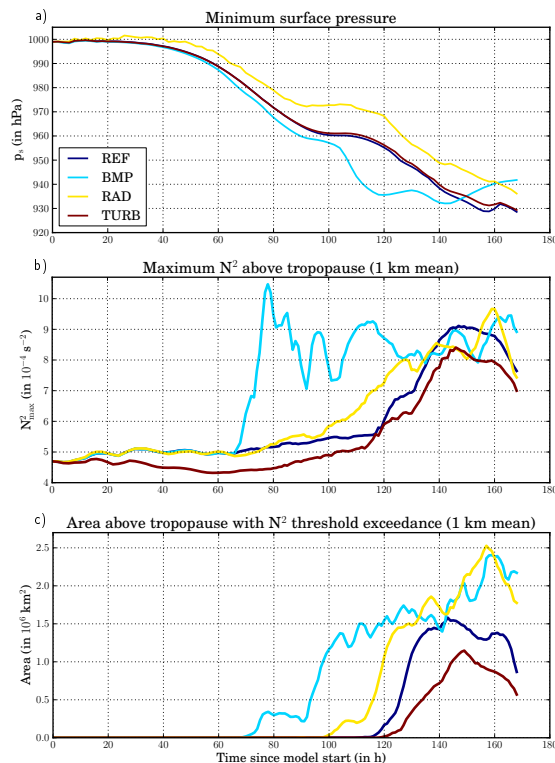


Figure 3. Temporal evolution over the entire simulated life cycles of **(a)** the minimum surface pressure p_s (in hPa), **(b)** the maximum static stability N^2_{max} (in $10^{-4} s^{-2}$) above the thermal tropopause, and **(c)** the area $A_{5.5}$ (in $10^6 km^2$) of N^2 threshold exceedance above the thermal tropopause (with a threshold of $N^2 = 5.5 \times 10^{-4} s^{-2}$). Dark blue lines show N^2_{max} of REF, light blue of BMP, yellow of RAD, and dark red of TURB.

TIL in baroclinic life cycle experiments

D. Kunkel et al.

Title Page

Abstract

Introduction

Conclusions

References

Tables

Figures



Back

Close

Full Screen / Esc

Printer-friendly Version

Interactive Discussion

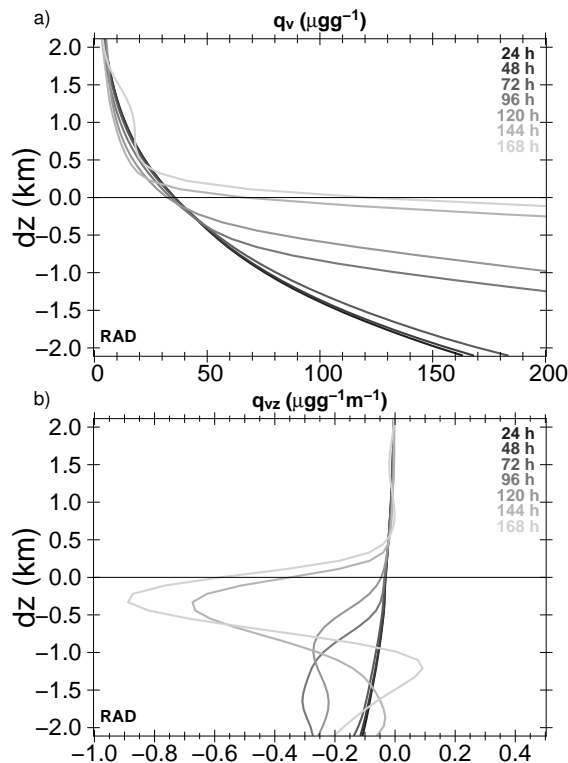


Figure 4. Instantaneous thermal tropopause based domain mean values of **(a)** specific humidity q_v (in $10^{-6} \text{ kg kg}^{-1}$) and **(b)** the vertical gradient of specific humidity $\partial q_v / \partial z$ (in $10^{-6} \text{ kg kg}^{-1} \text{ m}^{-1}$) for RAD. The domain mean is calculated within $25\text{--}65^\circ$ latitude and the entire zonal domain. The intensity of the gray colors indicates the time since model start in 24 h intervals.

TIL in baroclinic life cycle experiments

D. Kunkel et al.

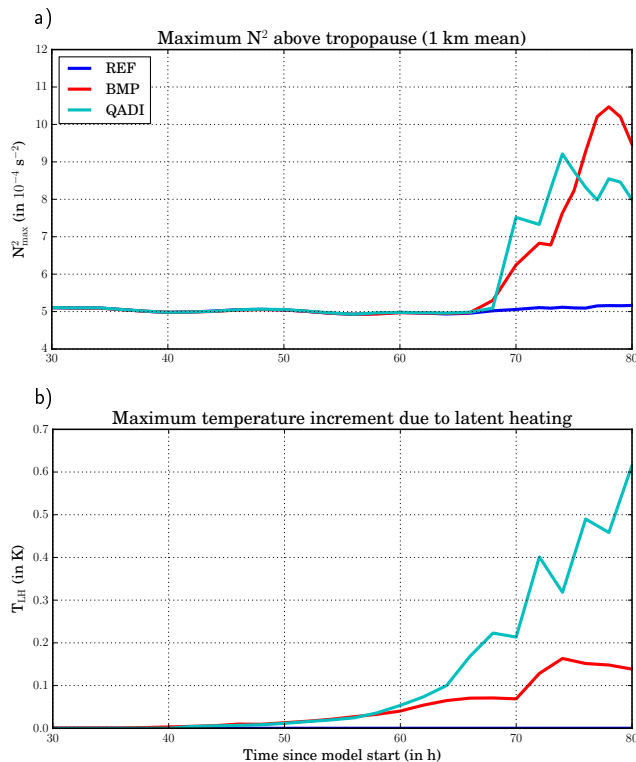


Figure 5. Temporal evolution over the entire simulated life cycles of **(a)** the maximum static stability N_{\max}^2 (in 10^{-4} s^{-2}) above the thermal tropopause and **(b)** the maximum temperature increment due to latent heating T_{LH} (in K) in the model domain for REF (blue lines), BMP (red lines), and QADI (cyan lines).

TIL in baroclinic life cycle experiments

D. Kunkel et al.

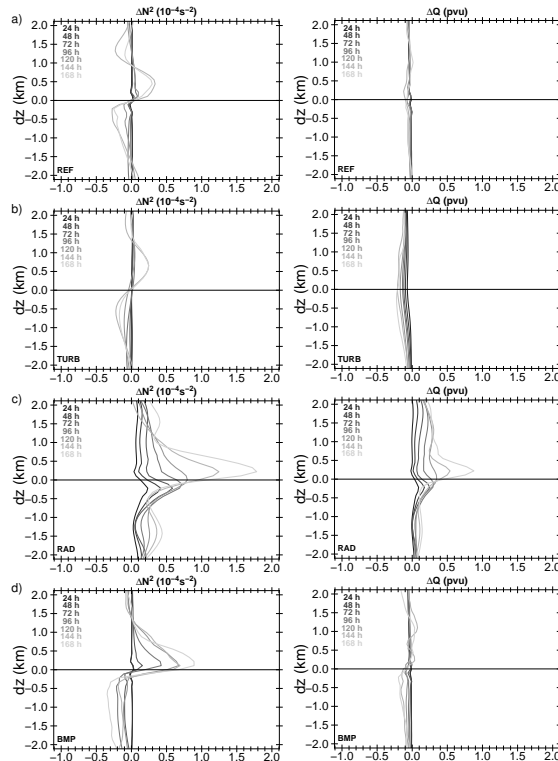


Figure 6. Instantaneous thermal tropopause based domain mean values of ΔN^2 (in 10^{-4} s^{-2}) in the upper row and ΔQ (in pvu) in the lower row for **(a)** REF, **(b)** TURB, **(c)** RAD, and **(d)** BMP. The domain mean is calculated within $25\text{--}65^\circ$ latitude and the entire zonal domain. The intensity of the gray colors indicates the time since model start in 24 h intervals. ΔN^2 is the difference between the current static stability N^2 and the advected initial static stability $\text{ADV}(N_0^2)$, ΔQ is the difference between the current potential vorticity Q and the advected initial potential vorticity $\text{ADV}(Q_0)$.

Title Page

Abstract

Introduction

Conclusions

References

Tables

Figures

◀

▶

◀

▶

Back

Close

Full Screen / Esc

Printer-friendly Version

Interactive Discussion



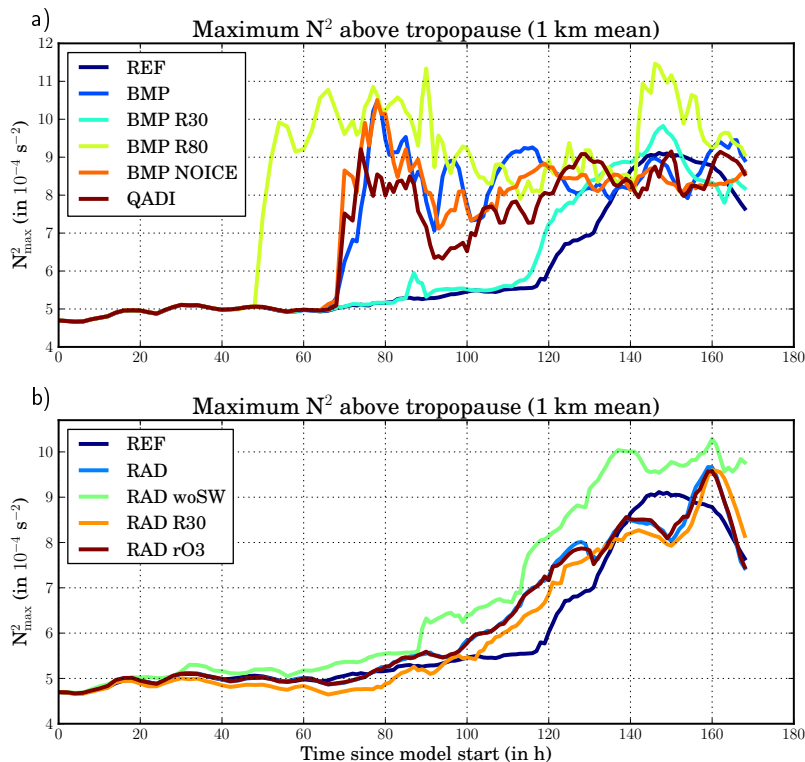


Figure 7. Temporal evolution of the maximum static stability N_{\max}^2 (in 10^{-4} s^{-2}) above the thermal tropopause for sensitivity simulations of (a) BMP and (b) RAD. In (a) N_{\max}^2 is shown for REF (dark blue), BMP (blue), BMP R30 (light blue), BMP R80 (green), BMP NOICE (orange), and QADI (dark red). In (b) N_{\max}^2 is shown for REF (dark blue), RAD (blue), RAD woSW (green), RAD R30 (orange), and RAD rO3 (dark red).

TIL in baroclinic life cycle experiments

D. Kunkel et al.

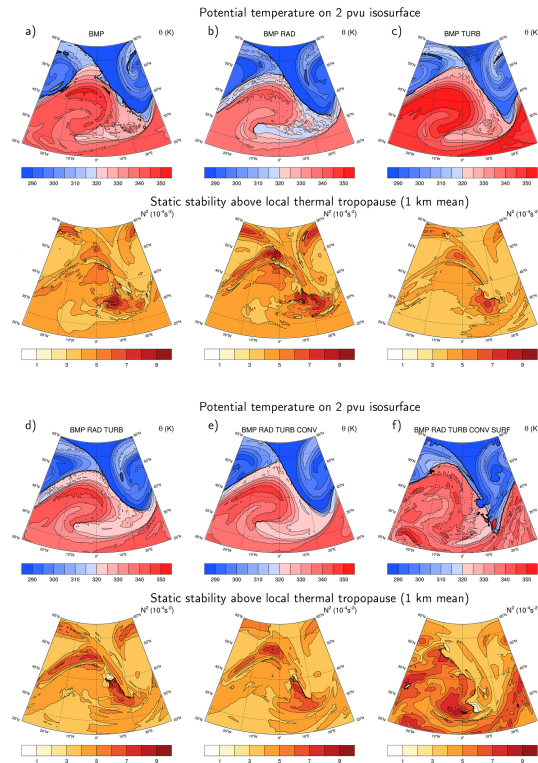


Figure 8. Dynamical and thermodynamical state of baroclinic life cycles after 120 h of model integration. In the upper rows of the six panels the distribution of potential temperature Θ (in K) on the dynamical tropopause is depicted, while the lower rows show the distribution of static stability N^2 (in 10^{-4} s^{-2}) averaged over the first kilometer above the thermal tropopause for (a) BMP, (b) BMP RAD, (c) BMP TURB, (d) BMP RAD TURB, (e) BMP RAD TURB CONV, and (f) BMP RAD TURB CONV SURF.

Title Page

Abstract

Introduction

Conclusions

References

Tables

Figures



Back

Close

Full Screen / Esc

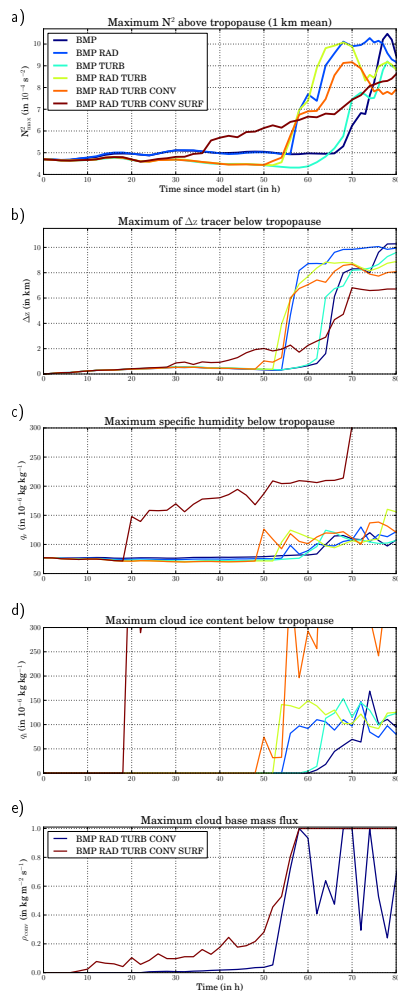
Printer-friendly Version

Interactive Discussion



TIL in baroclinic life cycle experiments

D. Kunkel et al.



Title Page

Abstract

Introduction

Conclusions

References

Tables

Figures



Back

Close

Full Screen / Esc

Printer-friendly Version

Interactive Discussion



Figure 9. Temporal evolution over the first 80 h of the life cycles of **(a)** N_{\max}^2 (in 10^{-4} s^{-2}) above the thermal tropopause, **(b)** the maximum of the Δz tracer (in km) in a 500 m thick layer below the thermal tropopause, **(c)** the maximum specific humidity q_v in a 500 m thick layer below the thermal tropopause (in $10^{-6} \text{ kg kg}^{-1}$), **(d)** the maximum specific cloud ice content q_i in a 500 m thick layer below the thermal tropopause (in $10^{-6} \text{ kg kg}^{-1}$), and **(e)** the maximum cloud base mass-flux ρ_{CONV} (in $\text{kg m}^{-2} \text{ s}^{-1}$). For **(a–e)** the colored lines indicate the following simulations: REF (dark blue), BMP (blue), BMP RAD (light blue), BMP TURB (green), BMP RAD TURB (yellow), BMP RAD TURB CONV (orange), and BMP RAD TURB CONV SURF (dark red). For **(f)** only the simulations with convection are considered: BMP RAD TURB CONV (dark blue) and BMP RAD TURB CONV SURF (dark red).

TIL in baroclinic life cycle experiments

D. Kunkel et al.

Title Page	
Abstract	Introduction
Conclusions	References
Tables	Figures
◀	▶
◀	▶
Back	Close
Full Screen / Esc	
Printer-friendly Version	
Interactive Discussion	



TIL in baroclinic life cycle experiments

D. Kunkel et al.

Title Page

Abstract

Introduction

Conclusions

References

Tables

Figures



Back

Close

Full Screen / Esc

Printer-friendly Version

Interactive Discussion

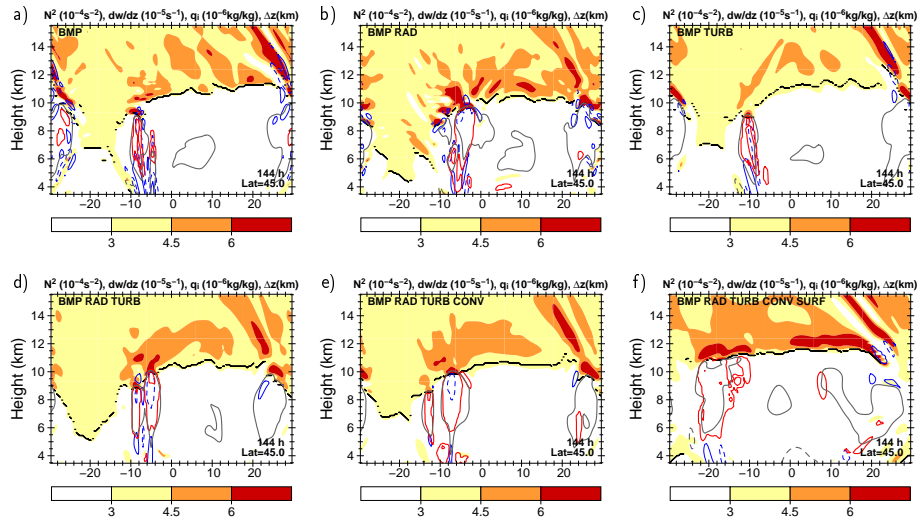


Figure 10. Zonal cross sections along 45° N of static stability N^2 (in 10^{-4} s^{-2}) after 144 h of model integration. Red lines show specific cloud ice content q_i (for $5.0 \times 10^{-6} \text{ kg kg}^{-1}$), solid blue lines show regions with positive values of $\partial w / \partial z$ (for $10.0 \times 10^{-5} \text{ s}^{-1}$), dashed blue lines show negative values (for $-10.0 \times 10^{-5} \text{ s}^{-1}$), and solid gray lines show regions with Δz tracer larger than 2.5 km. The thick black line is the thermal tropopause. The six panels show **(a)** BMP, **(b)** BMP RAD, **(c)** BMP TURB, **(d)** BMP RAD TURB, **(e)** BMP RAD TURB CONV, and **(f)** BMP RAD TURB CONV SURF.

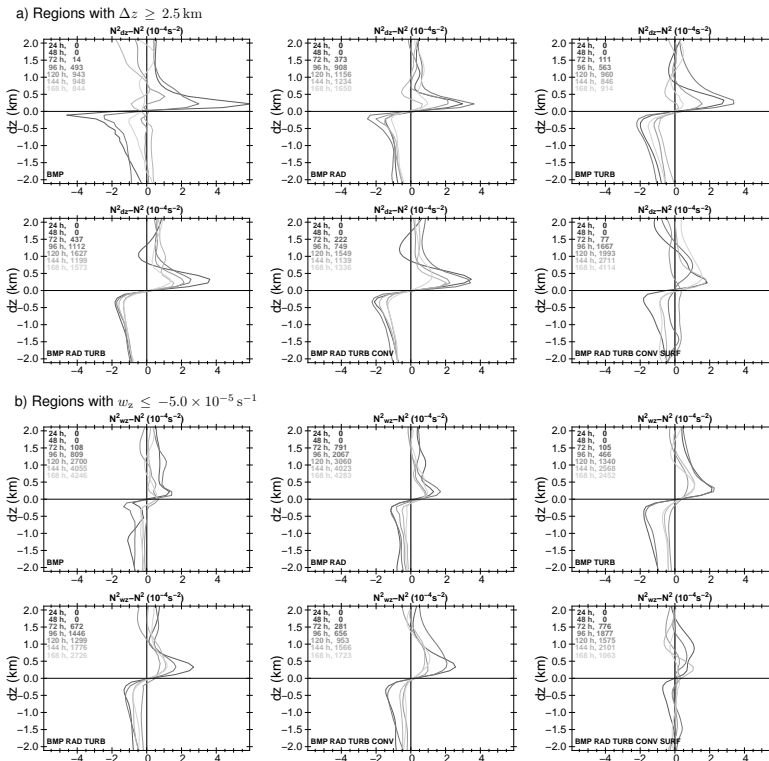


Figure 11. (a) Instantaneous thermal tropopause based vertical profiles of difference between the mean of static stability in regions with $\Delta z > 2.5$ km N_{dz}^2 and the domain mean N^2 (in 10^{-4} s^{-2}) for each 24 h of the model integration. (b) Differences for regions with $\partial w / \partial z \leq -5.0 \times 10^{-5} \text{ s}^{-1}$. The values in the top left corner of each panel show the number of individual profiles used for calculating the respective mean profile.

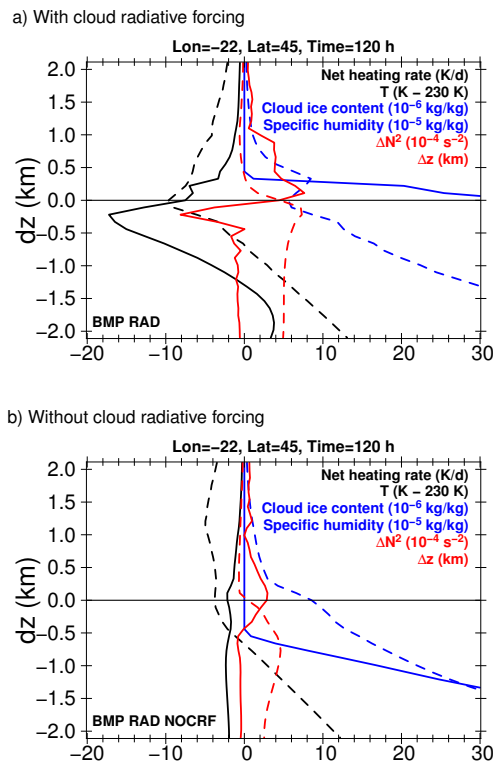


Figure 12. Tropopause based vertical profiles through an ice cloud along the central latitude at 120 h for (a) a simulation with cloud radiative forcing (BMP RAD) and (b) a simulation without cloud radiative forcing (BMP RAD NOCRF). Solid lines show net radiative heating (in $K d^{-1}$, scaled for better comparability, black), cloud ice content (in $10^{-6} \text{ kg kg}^{-1}$, blue), and ΔN^2 (in 10^{-4} s^{-2} , red). Dashed lines show temperature (in $K - 230 K$, black), specific humidity (in $10^{-5} \text{ kg kg}^{-1}$, blue), and Δz (in km , red).

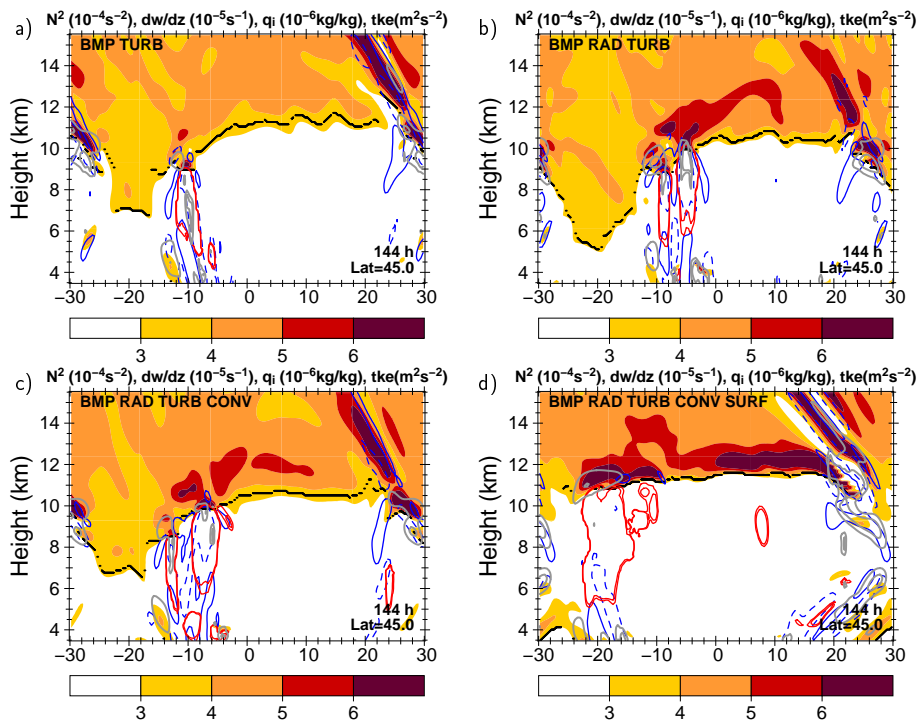


Figure 13. Zonal cross sections along 45°N of static stability N^2 (in 10^{-4} s^{-2}) after 144 h of model integration. Solid blue lines show regions with positive values of the vertical divergence $\partial w / \partial z$ (for 5.0, $50.0 \times 10^{-5} \text{ s}^{-1}$), dashed blue lines show negative values (for -5.0 , $-50.0 \times 10^{-5} \text{ s}^{-1}$). Red lines show specific cloud ice content q_i (for 5.0, $10.0 \times 10^{-6} \text{ kg kg}^{-1}$). Gray lines show turbulent kinetic energy (TKE) (in 0.5, 1.0, $5.0 \text{ m}^2 \text{ s}^{-2}$). The four panels show (a) BMP TURB, (b) BMP RAD TURB, (c) BMP RAD TURB CONV, and (d) BMP RAD TURB CONV SURF.